Positron annihilation at proton-induced defects in 6*H*-SiC/SiC and 6*H*-SiC/SiO_2/Si structures

M.-F. Barthe, L. Henry, C. Corbel, and G. Blondiaux
Centre d'Etudes et de Recherches par Irradiation, Centre National de la Recherche Scientifique, 3A rue de la Férollerie, 45071 Orléans, France

K. Saarinen and P. Hautojärvi
Laboratory of Physics, Helsinki University of Technology, 02150 Espoo, Finland

E. Hugonnard and L. Di Cioccio
LETI-CEA, Département de microtechnologies, 17 avenue des martyrs, 38054 Grenoble Cedex, France

F. Letertre and B. Ghyselen
SOITEC, Parc des fontaines 38, 190 Bernin, France
(Received 24 March 2000)

Positron annihilation is used to detect vacancy-related defects in proton-implanted and Smart Cut 6*H*-SiC. The measurement of positron-electron pair momentum distribution as a function of depth shows that vacancy-related defects produced along the proton track and cavities formed in the region of the hydrogen peak survive in smart cut 6*H*-SiC even after 1300 °C annealing.

I. INTRODUCTION

The Smart Cut process is an original method developed at LETI (Grenoble) to form silicon on insulator (SOI) material.[1,2] This process, combining hydrogen implantation and direct wafer bonding, has been adapted to be used for silicon carbide material[3,4] to construct SiC/SiO_2/Si structures (SiCOI) and provides a solution to form high-quality, low-cost 6*H*- or 4*H*-SiC/SiO_2/Si structures on $\geqslant$100 mm large Si wafers. The use of a 100-mm silicon substrate is of prime importance, since these substrates are cheap compared to the SiC substrates and allow access to the facilities commonly used for silicon processing. In addition, the other advantages are: the small thickness dispersion of the upper thin layer, the possibility of modulating the thickness of the SiC and oxide layers and the recycling of the SiC wafer.

When the Smart Cut process is applied to *n*-type 6*H*-SiC epilayers or wafers, a partial compensation of the donor activity in 6*H*-SiC takes place, and annealing at high temperatures is required to recover the donor activity. This suggests that the defects induced by hydrogen implantation play a role in the compensation. To understand better which type of defect is involved in the compensation, their spatial distribution and annealing properties need to be characterized. In this paper, we focus on vacancy-type-related defects created along the proton track in 6*H*-SiC and Smart Cut 6*H*-SiC. We investigate these defects by measuring positron-annihilation characteristics as a function of depth before and after proton implantation, with or without Smart Cut processing.

II. EXPERIMENTAL DETAILS

The positron-annihilation experiments were performed with a slow-positron beam at the Helsinki University of Technology in eight differently processed 4-μm (six) and 1-μm (2) thick, [1000] 6*H*-SiC CREE layers. The beam was magnetically guided and delivered monoenergetic positrons with energy varying from 0.1 to 25 keV. The positron mean implantation depth in 6*H*-SiC varies from 0.18 nm to 2.2 μm in this energy range. The 6*H*-SiC crystals were grown by chemical vapor deposition (CVD) on 6*H*-SiC substrates with nitrogen doping used to obtain electron concentrations of $10^{17}\,cm^{-3}$ in layers and $3.5\times10^{18}\,cm^{-3}$ in substrates. Three 4-μm-thick 6*H*-SiC/SiC layers were left in their as-grown state (see Table I). Three 4-μm-thick 6*H*-SiC(H)/SiC layers were implanted with protons in the 4×10^{16}-cm^{-2} range and then exhibited *n*-type conduction by a hopping mechanism. One of them, called Hai, is used as the reference as-implanted sample. The others were annealed at 900 °C (*H*900, SI-type) and 1300 °C (*H*1300, SI-type). The two last 1-μm-thick layers, 6*H*-SiC(*H*sc)/SiO_2/Si, went through all the stages of the Smart Cut process and one of them was further annealed at 1300 °C to remove partial compensation.

The Smart Cut (sc) process[1] uses two thermally oxidized SiO_2(0.5 μm)/6*H*-SiC/SiC and SiO_2(0.5 μm)/Si structures to produce the final 6*H*-SiC(*H*sc)(1 μm)/SiO_2/Si multilayer structures. The SiO_2(0.5 μm)/6*H*-SiC/SiC structure is implanted with protons at a high fluence of $8\times10^{16}\,cm^{-2}$. The protons go through SiO_2 and stop 1 μm deep in 6*H*-SiC. After implantation, thermal bonding is achieved between the SiC/6*H*-SiC(H)/SiO_2(H) and the SiO_2/Si structures. Then, the 6*H*-SiC(H) layer is fractured in the region of the proton peak by annealing at 900 °C. The fracture results from a high concentration of large vacancy-type defects that form in the proton peak region during 900 °C annealing and are described as platelets in Refs. 1–3.

The result is a 6*H*-SiC(*H*sc)(1 μm)/SiO_2(1 μm)/Si structure where, in the 6*H*-SiC(*H*sc), the fractured proton peak region is near the surface and the region through which the protons went extends up to the SiO_2 layer. One notices

TABLE I. Characteristics of the 6*H*-SiC layers before and after proton implantation.

Structure	Type	Label	Doping (cm^{-3}) *n* type Epi. ($\times 10^{17}$)	Doping (cm^{-3}) *n* type Subs. ($\times 10^{18}$)	H^+ implantation ($10^{16}\,cm^{-2}$) ($R_p = 1\ \mu m$)	Annealing Temp. (°C)
6*H*-SiC/SiC	As grown	ref1	1	3.5		
	As grown	ref2	1	3.5		
	As grown	ref3	1	3.5		
6*H*-SiC(H)/SiC	As implanted	Hai	1	3.5	~4	
	Implanted and annealed	H900	SI		~4	900
		H1300	SI		~4	1300
6*H*-SiC(*H*sc)/SiO_2/Si	As fractured	SiCOI900	SI		>4	900
	Annealed	SiCOI1300	SI		>4	1300

therefore that, in 6*H*-SiC(*H*sc), the proton stopping power decreases as the depth increases. One can assume that the spatial distribution of defects calculated with SRIM98 in the 6*H*-SiC(*H*sc) [Fig. 1(b)] layer is roughly symmetric to that in the 900 °C 6*H*-SiC(H) layer [Fig. 1(a)] in a planlike symmetry, where the plan is located at about half of the proton track. The fluences in the layers 6*H*-SiC(*H*sc) and 6*H*-SiC(H) differ by a factor of 2 due to the concentration of hydrogen necessary to induce the fracture at 900 °C in 6*H*-SiC(*H*sc).

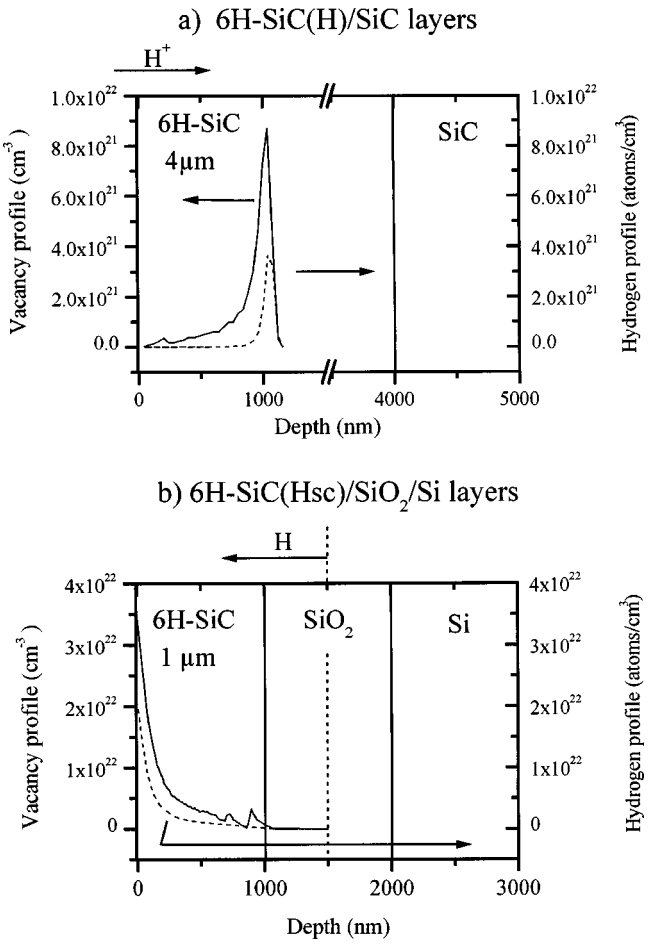

FIG. 1. Calculations using SRIM98 (Ref. 10) of the hydrogen and vacancy profiles created by proton implantation in (a) the 6*H*-SiO(H)/SiC structure and (b) the 6*H*-SiC(*H*sc)(1 μm)/SiO_2/Si Smart Cut structure. The vacancy calculated profiles do not take into account the vacancy diffusion, recombination, or agglomeration occurring during implantation or the 900 or 1300 °C annealing.

The positron-annihilation characteristic that was investigated is the positron-electron pair momentum distribution. It was measured at 300 K by recording the Doppler broadening of the 511-keV annihilation line with a Ge detector [full width at half maximum (FWHM) 1.2 keV at 511 keV)]. Approximately 10^6 events were collected in the peak at each positron energy value. The window 511[−6.98;+6.98] keV was used to calculate the total number of annihilation events (N_A). The broadening of the annihilation γ line, ΔE_γ, is proportional to the momentum component of the annihilating electron-positron pair, p_L, along the emission direction of the photons: $2\Delta E_\gamma = cp_L$. Two parameters are used to characterize the shape of the momentum distribution. The low-momentum parameter S in the window at the peak, 511[−0.73;+0.73] keV, corresponds to the fraction of annihilations taking place in the momentum range $(0 - |2.88|) \times 10^{-3} m_0 c$. The high-momentum parameter W in the windows at the wings, 511[−6.98;−2.70] keV and 511[+2.70;+6.98] keV, corresponds to the fraction of annihilations taking place in the momentum range $(|11.27| - |27.32|) \times 10^{-3} m_0 c$.

To investigate the depth dependence of S and W, the curves $S(E)$ and $W(E)$ were recorded as a function of the beam energy E changed in 0.5-keV steps. At a given energy, $S(E)$ and $W(E)$ are averages of the annihilation characteristics at the 6*H*-SiC surface in the 6*H*-SiC layer and, for the Smart Cut structure, in the SiO_2 and Si layers weighted by the corresponding annihilation fractions $fj(E)$. To determine whether only two distinct annihilation characteristics contribute to a set of data (S,W) in a given energy range, we use the graphical analysis[5] where S is plotted as a function of W with the energy E as running parameter. When only two distinct annihilation characteristics (S_1,W_1) and (S_2,W_2) contribute, the $S(W)$ plot falls on a segment of a straight line that is a fingerprint of the superposition of the two annihilation characteristics and goes from (S_1,W_1) $(f_1=1)$ to (S_2,W_2) $(f_2=1)$. This property of the $S(W)$ plot has been earlier successfully used for defect investigation in layers or bulk.[5]

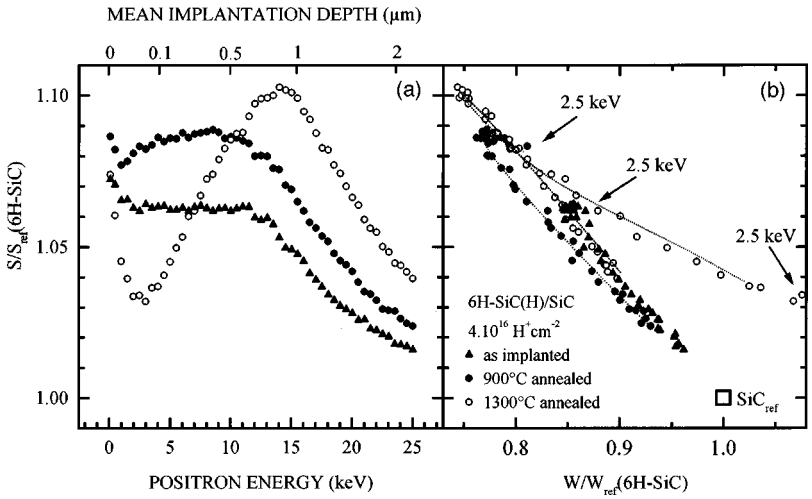

FIG. 2. (a) Low-momentum fraction $S=N_A([0-|2.88|]\times10^{-3}m_0c)/N_A([0-|27.32|]\times10^{-3}m_0c)$ as a function of positron beam energy and (b) as a function of high-momentum fraction $W=N_A([|11.27|-|27.32|]\times10^{-3}m_0c)/N_A([0-|27.32|]\times10^{-3}m_0c)$ in H^+-implanted SiC(H)/SiC layers annealed at 900 or 1300 °C. The mean implantation depth in SiC is $z(E)\,[\mathrm{nm}]=9.17E^{1.7}\,[\mathrm{keV}]$ (Ref. 25). A modified version of VEPFIT (Ref. 6) is used to consistently fit (dotted lines) the $S(W)$ curves from 2.5 keV in the annealed layers.

The $S(E)$ curves as a function of positron energy in Fig. 2(a) show a strong discontinuity around 2.5 keV. All the other $S(E)$ or $W(E)$ curves exhibit a similar feature. This discontinuity marks the beginning of the energy region where the positron distribution in the sample is governed by implantation and diffusion. This will be detailed elsewhere by examining the variation of the positronium-annihilation fraction in the 6*H*-SiC samples as a function of positron energy. Hereafter, a modified version of VEPFIT[6] is used to consistently fit the $S(E)$ and $W(E)$ curves from 2.5 keV and the data below 2.5 keV are discarded.

III. DATA ANALYSIS

A. 6*H*-SiC/SiC

The three as-grown 6*H*-SiC layers give reproducible results. $S(W)$ decreases (increases) as a function of positron energy from 2.5 keV up to 15 keV and then remains constant up to 25 keV. The $S(W)$ plots above 2.5 keV form a segment of straight line. This property indicates that above 2.5 keV annihilation results from the mixing of only two annihilation characteristics, the surface and the 6*H*-SiC characteristics. The fitting of the data in the layers leads to a positron effective diffusion length of $l^+=200$ nm and annihilation characteristics in the layers equal to the values measured on the plateaus between 15 and 25 keV with $(S_{\mathrm{ref}},W_{\mathrm{ref}})=(0.4526(5),0.0416(3))$. The substrates where electron concentration is a factor 30 higher than in the layers give the same annihilation characteristics as the layers. We propose that these annihilation characteristics, which are independent on the electron concentration, correspond to those in the 6*H*-SiC lattice. When compared to the values found in Si, the effective diffusion length we determine in these 6*H*-SiC CREE materials is comparable to the diffusion length reported for the Si lattice.[7] It is however much longer than that determined by Brauer *et al.*[8] in 6*H*-SiC *n*-type wafers. Consistently, the ratio $S(\mathrm{Si})/S(6H\text{-SiC})=1.15$ we obtain is higher than the ratio of 1.049 obtained by these authors. It can be noticed that Dannefaer, Puff, and Kerr[9] measured a value for this ratio that is about the same as we did in the *n*-type (N-doped) SiC sample.

6H-SiC(H)/SiC after implantation

After correction from the surface contribution, the positron characteristics in the three hydrogen implanted layers differs strongly from those measured in the reference layer. Figure 2 shows that, at 25 keV, where the surface contribution has vanished, all the *S* values are higher in the implanted layers than in the as-grown layers, whereas all the *W* values are lower. This indicates that proton implantation has introduced vacancy-related defects that survive up to 1300 °C at least. None of the $S(W)$ plots above 2.5 keV consist of a segment of straight line running over the total energy range. This provides evidence that the spatial distribution of defects ''seen'' by positrons is inhomogeneous in concentration and/or in type as a function of depth. Some parts of the distribution can, however, be assimilated to segments of straight line. In this energy range, a crude model can be applied where, in a first approximation, it is assumed that the distribution seen by positrons is homogeneous.

As shown in Fig. 1, the profile of vacancy distribution created by protons along their tracks can be calculated by using SRIM98.[10] It shows that, when defect recombination and migration is ignored, the number of vacancies along the track is nearly constant and displays a peak in the narrow region located approximately at 1 μm, where defect cascade due to hydrogen stopping occurs. Such a distribution suggests to check first whether the $S(W)$ plot and the fitting in each sample can be consistent with the existence of three regions corresponding to the track region (*T*), the cascade region (*C*) and the beyond cascade region (BC). For each region, the parameters of the fitting are its width, the positron diffusion l_i^+ and the constant annihilation characteristics S_i and W_i. A further simplification in the model can be introduced by noticing that the $S(W)$ plots in Fig. 2(b) above 12.5 keV in Hai, 17 keV in *H*900, and 14.5 keV in *H*1300 samples exhibit a segment of line going through the annihilation characteristics in as-grown 6*H*-SiC. Such plots are consistent with BC regions where the annihilation characteristics are the same as before implantation. In the fittings, the positron effective diffusion length in the BC regions was constrained to the value $l^+=200$ nm determined in as-grown 6*H*-SiC. We examine below the details of such fittings.

After proton implantation, the $S(W)$ plot in the sample Hai [Fig. 1(b)] is consistent with the existence of a track

region where the annihilation characteristics are given by the values $(S_{\mathrm{Tai}}, W_{\mathrm{Tai}}) = (0.4819(4), 0.0353(2)) = (1.064, 0.850) \times (S_{\mathrm{ref}}, W_{\mathrm{ref}})$, where the two segments of straight line forming the $S(W)$ plot cross. To obtain a good fitting in this model, the track region must extend up to 0.9 μm at least and the nonimplanted region starts beyond 1.075 μm. The fits are better when a cascade region is included but the values in this region are strongly depending on its width. For a given width of 175 nm starting at 0.9 μm as suggested by SRIM98 calculations, the values are $(S_{\mathrm{Cai}}, W_{\mathrm{Cai}}) = (0.4953, 0.0300)$.

After 900 °C annealing, one can define two energy ranges for the variations of S or W. In Fig. 2(a), S in the $H900$ sample goes through a broad faint maximum between 5 to 12.5 keV and, then, from 12.5 to 25 keV, decreases strongly. In the same energy ranges, W [Fig. 2(b)] varies in opposite ways to S: W goes first through a broad minimum and then increases strongly. Good fittings can be achieved with a model where the width of the track region in the $H900$ sample is constrained to the values determined in the Hai sample and the width of the cascade region is increased up to 1.19 μm. In the track region, it is possible to constrain the values S_{T900} and W_{T900} to the values of the point where, in Fig. 2(b), the two segments of straight line start immediately on each side of the maximum. The best fitting is obtained for $(S_{T900}, W_{T900}) = (0.4924(4), 0.0318(2)) = (1.078, 0.766)$ $(S_{\mathrm{ref}}, W_{\mathrm{ref}})$. These values are quite close to the extrema measured at 8 keV, $S_{H900\,\max} = 1.086\, S_{\mathrm{ref}}$ and $W_{H900\,\min} = 0.768\, W_{\mathrm{ref}}$. In the cascade region, for a width of 219 nm starting at 0.9 μm, the (S_{C900}, W_{C900}) values are (0.4906(20), 0.0308(4)) close to the cascade values in the Hai sample.

After 1300 °C annealing, S in sample $H1300$ [Fig. 2(a)] varies strongly as a function of energy. S goes through a sharp maximum at 14 keV while W goes through a sharp minimum. The $S(W)$ plot shows that the material is inhomogeneous in the proton track region. It indicates that the defects either are in lower concentration near the surface than deeper in the sample or change of type as a function of depth. It also suggests that, in the deeper layer of the track region, the defects give annihilation characteristics close to S_{T900}, and W_{T900}. The quality of the fittings is rather insensitive to the inclusion or not of an extra layer near the surface. It is much more sensitive to the width of the cascade region, which needs to be extended up to 1.3 μm at most. A good fitting has been obtained for a track region divided into two regions: a narrow near surface region up to 0.31 μm where (S_{1300}, W_{1300}) are (0.476, 0.0362) followed by a broader region finishing at 1.05 μm with $(S_{T1300}, W_{T1300}) = (0.4945(5), 0.0319(2)) = (1.092, 0.766)$ $(S_{\mathrm{ref}}, W_{\mathrm{ref}})$. The cascade has a width of 240 nm with $(S_{C1300}, W_{C1300}) = (0.565(2), 0.0172(5))$. The fitted values in the cascade region are quite far from those fitted in Hai and $H900$ samples and from the extrema measured at 14 keV (Fig. 1) $S_{H1300\,\max} = 1.102\,71\, S_{\mathrm{ref}}$ and $W_{H1300\,\min} = 0.743\,75\, W_{\mathrm{ref}}$. The fitting is better when a weak electric field of 250 V/cm is applied in the BC region starting at 1.29 μm and pushes the positrons deeper in the layer.

B. 6*H*-SiC(*H*sc)/SiO$_2$/Si

The $S(E)$ and $W(E)$ plots in the as-fractured 6H-SiC(Hsc)/SiO$_2$/Si structure (SICOI900) in Fig. 3 exhibits three regions of variations beyond the near-surface region. In the first region, from about 2.5 keV up to 10.5 keV, S and W reach values that are quite close to the S_{T900} or W_{T900} fitted values in sample $H900$. From 10.5 to ~15 keV, S and W both exhibit an increase. From ~15 to 25 keV, S goes on increasing while the W behavior changes with W decreasing deeply. One notices that in all regions, except in the 10.5–15-keV region, the variations of S and W are in opposite directions. One can also observe that, after 1300 °C annealing, the $S(E)$ and $W(E)$ plots have this striking feature, with the variations of S and W in the same directions only in the 10.5–15-keV region. This feature indicates that positrons annihilate in a multilayer structure.

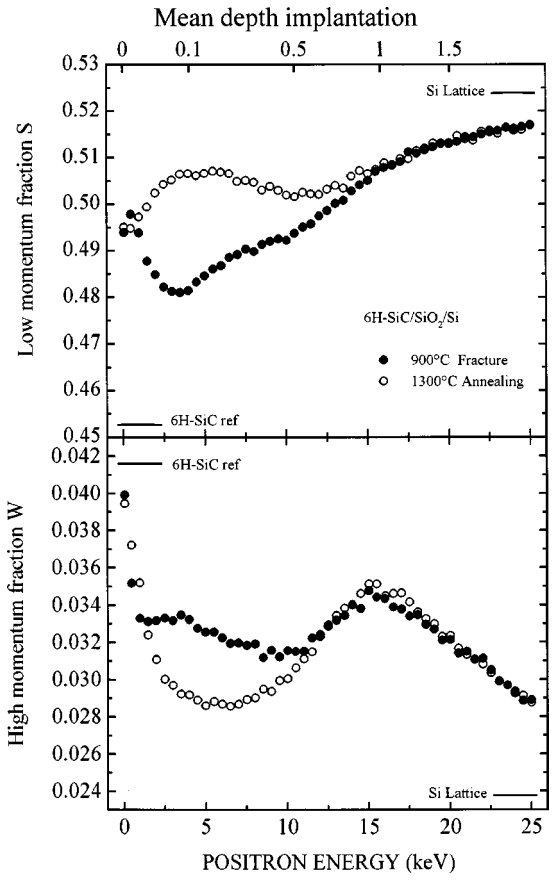

FIG. 3. (a) Low-momentum fraction $S = N_A([0 - |2.88|] \times 10^{-3} m_0 c)/N_A([0 - |27.32|] \times 10^{-3} m_0 c)$ and (b) high-momentum fraction $W = N_A([|11.27| - |27.32|] \times 10^{-3} m_0 c)/N_A([0 - |27.32|] \times 10^{-3} m_0 c)$ in the 6H-SiC(Hsc)SiO$_2$/Si structures produced by Smart Cut directly after 900 °C fracture or after 1300 °C annealing as a function of positron beam energy.

One can easily determine the layers where positron annihilate by examining the $S(W)$ plot in the 6H-SiC(Hsc)/SiO$_2$/Si structures (Fig. 4) with energy E as the running parameter. This plot can be decomposed into three segments of straight line corresponding to the three energy ranges 2.5–10.5, 10.5–15.5, and 15.5–25 keV, which are the same as those defined in the $S(E)$ and $W(E)$ plots (Fig. 3). The two first segments below 15.5 keV change strongly after annealing, whereas the third one, from 18–19 to 25 keV, remains unchanged. This last segment goes through the Si lattice point with $S(W)$ increasing (decreas-

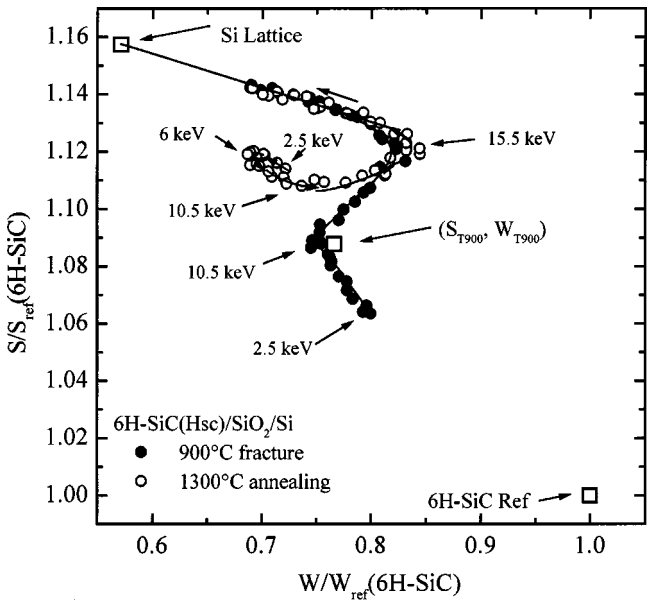

FIG. 4. Annihilation characteristics in the 6*H*-SiC(*H*sc)/SiO_2/Si structures produced by Smart Cut directly after 900 °C fracture or after 1300 °C annealing: low-momentum fraction S/S_{ref} as a function of the high-momentum fraction W/W_{ref}. The solid lines are guides to the eye. The values in parentheses correspond to 6*H*-SiC reference, Si lattice, and to the annihilation characteristics (S_{T900}, W_{T900}) of the defects produced in the track region after 900 °C annealing in proton-implanted 6*H*-SiC(H)/SiC.

ing) to the Si lattice $S(W)$ value. One can easily attribute the segments successively to annihilations in 6*H*-SiC(*H*sc), then in 6*H*-SiC(*H*sc) and SiO_2 and, finally, in SiO_2 and Si. After the 900 °C fracture, the surface contribution fades out above 7 keV. From 7 to 10.5 keV, where the S or W values are nearly constant and quite close to the S_{T900} or W_{T900} fitted values in sample *H*900, it is likely that positrons annihilate mainly in the 900 °C track defects. After 1300 °C annealing, there is a strong contribution of the cascade defects to positron annihilation in 6*H*-SiC(*H*sc). It is combined with annihilation at the surface from 2.5 to ~7 keV. It is combined with annihilation at the track defects from ~7 to 10.5 keV.

IV. DISCUSSION: PROPERTIES OF DEFECTS IN THE TRACK AND CASCADE REGION

The huge changes induced by 900 °C annealing in the annihilation characteristics along the proton track indicate that the nature of the vacancy-related defects that trap positrons changes under 900 °C annealing. To discuss the nature of the defects along the track before and after annealing, we need to question whether the S_{Tai}, W_{Tai}, and S_{T900}, W_{T900} characteristics correspond to positrons fully trapped in an unique type of defects or in a mixing of defects. We document below this question.

In recent years, defects have been widely investigated in ion or electron irradiated SiC using a variety of techniques, especially in the cubic 3*C*-SiC polytype (see references in Ref. 12). In this last polytype, Si or C vacancies occupy only one type of site. The situation is more complicated in 6*H*-SiC, where the stacking sequence of the tetrahedrally bonded Si/C bilayers changes from zinc blende (cubic) to wurtzite (hexagonal) in adjacent bilayer planes. This leads to the existence of three inequivalent sites for the Si and C atoms, one hexagonal and two cubic sites and, consequently, to three inequivalent Si or C vacancies. Vacancy clustering then leads to divacancy, trivacancy, and *n*-vacancy clusters with a variety of inequivalent configurations. In SiC samples where vacancies at inequivalent sites coexist, it can be difficult to resolve the positron characteristics at each site. It may be achieved in samples specially designed, once it has been clearly demonstrated that, as suggested by some authors,[11] the charge state or the recovery properties of inequivalent sites differ significantly. Comparing previous EPR results[11] with their deep-level transient spectroscopy[12] (DLTS) results, Aboelfotoh and Doyle have proposed that, after low fluence ($\leqslant 10^{16}\,\mathrm{cm}^{-2}$) 2-MeV electron irradiation or ($10^{11}\,\mathrm{cm}^{-2}$) 300-keV deuterium implantation, the C vacancy has a positive and two negative sites in *n*-type 6*H*-SiC that recover at about 200–300 and 1400 °C, respectively. They also propose that the Si vacancy occupies two negative sites and recover over a broad range from 200 to 800 °C. The energy levels $E_c-0.62$ eV and $E_c-0.64$ eV they attribute to the Si vacancy have been, however, earlier attributed to the divacancy V_{Si}-V_{C} on nearest-neighbor sites with C_{3v} symmetry and were found to survive up to 1700 °C.[13] A zero-phonon line at 1.973 eV revealed by photoluminescence in electron- or ion-irradiated 6*H*-SiC and surviving up to 1700 °C was also earlier associated with a divacancy.[13–15] These quotations to published work clearly show that further work is required to firmly identify the nature of the defects produced by electron or ion implantation in SiC.

After implantation at low fluence (Hai sample), the values S_{ai} and W_{ai} are just slightly above the values we measure after implantation at a fluence 20 times smaller than the present fluence. The value $S_{\mathrm{Tai}}/S_{\mathrm{ref}}=1.064$ differs by less than 1% from the value $S/S_{\mathrm{ref}}=1.055$ determined by Brauer *et al.* in initially *n*-type 6*H*-SiC after 200-keV (80-nm) Ge implantation in the fluence range $(3-30)\times 10^{16}\,\mathrm{cm}^{-2}$.[16] This leads us to attribute the values S_{Tai}, and W_{Tai} to fully trapped positrons. This proposal is consistent with the evidence of full trapping given by positron lifetime spectra measured by Brauer *et al.* and several other authors in 6*H*-SiC after ion implantation or electron irradiation and annealing at room temperature.[17–19] According Puff *et al.*,[19] positrons in initially $n=6.2\times 10^{18}\,\mathrm{cm}^{-3}$ N-doped 6*H*-SiC are found to be fully trapped after 5-MeV proton implantation at $T\leqslant 220$ K at a fluence of $10^{16}\,\mathrm{cm}^{-2}$ and room-temperature annealing. The same evidence is reported after 2- and 2.5-MeV high-fluence electron irradiation[18,17] in initially $n\geqslant 5.4\times 10^{17}\,\mathrm{cm}^{-2}$ N-doped 6*H*-SiC.

The Doppler data suggest that the S_{Tai} and W_{Tai} values correspond to positrons fully trapped in a unique type of defect or in a mixing of defects where the relative trapping rates are weakly dependent on the fluence or ion nature. According to Brauer *et al.*, the lifetime spectra associated with the value $S/S_{\mathrm{ref}}=1.055$ can be decomposed into two components. Each of them correspond to positrons trapped at vacancy-type defects. The longest lifetime is around 235 ps, which, according theoretical lifetimes in SiC,[20] is too high for monovacancies and suggest rather divacancies or small vacancy clusters. The three other lifetime studies[19,18,17] men-

tioned above reach also the conclusion that positrons are fully trapped in different type of defects after 5-MeV proton or electron irradiation in initially $n > 5.4 \times 10^{17}\,\mathrm{cm}^{-2}$ N-doped SiC. Polity, Huth, and Hausmann[18] show that after high-fluence electron irradiation ($\geqslant 10^{18}\,\mathrm{cm}^{-2}$) monovacancies and divacancies trap fully positrons after 90-K annealing. After annealings above 25 °C, monovacancies start to disappear and two substages can be separated from 25 to 230 °C and 230 to 480 °C. Above and up to 1130 °C, positrons are fully trapped at negative ions and divacancies. According these results, at 25 °C, positrons ''see'' a mixing of monovacancies and divacancies. It is therefore likely that the S_{Tai} and W_{Tai} values correspond to a mixing of defects. The values $(S_{\mathrm{Tai}}/S_{\mathrm{ref}}, W_{\mathrm{Tai}}/W_{\mathrm{ref}}) = (1.064, 0.85)$ are of the order of those[21] assigned to the divacancies in Si $(S_V 2/S_{\mathrm{Si}}, W_V 2/W_{\mathrm{Si}}) = (1.052, 0.78)$ and we propose that this reflects a high trapping fraction in the nearest divacancies.

The mixing of monovacancies and divacancies may reflect that, depending on their nature (Si or C) or sites, monovacancies have different migration energies. It may also reflect that nitrogen dopants partially determine the defect distribution after electron or ion irradiation. Nitrogen dopants can interact with some of the monovacancies migrating at low temperature ($\leqslant 90$ K) and stabilize them into nitrogen-vacancy complex up to much higher temperatures than their migration temperature. This is well-known to be the case for the phosphorus-vacancy[22] or oxygen-vacancy complex in Si, which is stable well above the V_{Si} migration temperature (≈ 70 K). Our 6*H*-SiC material, where *n* is at least 5 times smaller than that in the SiC materials used in Refs. 18 and 19, may contain 5 times less nitrogen than these materials.[18,19] If this is the case, the fraction of the stabilized nitrogen-monovacancy complex is possibly much lower in our samples than in heavily doped samples.

After 900 °C annealing, the Doppler data show that, in the track region, a new type of vacancy-type defect is produced. The changes in *S* and *W* indicate that the 900 °C defect has a bigger open volume than the divacancy detected on the as-implanted reference. Compared to the lattice, the variations ΔS_{T900} and ΔW_{T900} induced by this defect give a ratio $\Delta S_{T900}/\Delta W_{T900}$, which is smaller than that induced by the defect detected on the as-implanted reference in the track region. According to theory, when the open volume of a vacancy cluster increases from 1 to 5 vacancies in Si;[23] this ratio is always increasing. In 6*H*-SiC, where calculations are still missing, we suggest that the decrease of the ratio after 900 °C annealing reflects a change in open volume and chemical nature of the neighboring atoms of the dominant vacancy-cluster trapping positrons. The variation of *W* relative to *S* is bigger, indicating that the neighboring atoms in the 900 °C vacancy clusters give a lower contribution than that in the as-implanted ones. This suggests that around the 900 °C vacancy clusters there are more C atoms than around the vacancy clusters observed in the as-implanted sample. As seen above, one can consistently explain the 900 °C data in 6*H*-SiC(*H*sc) and in 6*H*-SiC(H) by proposing that positrons annihilate with the same characteristics in the track region. The proton fluence in 6*H*-SiC(*H*sc)/SiO_2/SiC is twice that in 6*H*-SiC(H), which suggests that the S_{T900} and W_{T900} values correspond most likely to fully trapped positrons. The trapping occurs either in a unique type of defects or in a mixing of defects where the relative trapping rates are independent of the fluences. The second possibility seems more likely since the full recovery study performed by Puff *et al.*[19] in initially SiC ($n > 1.7 \times 10^{18}\,\mathrm{cm}^{-2}$) suggests that there is a mixing of defects after 5-MeV proton implantation at $10^{16}\,\mathrm{cm}^{-2}$ and 900 °C annealing. Their study indicates that the 900 °C annealing temperature falls in a recovery domain where *S* and *W* varies, whereas the lifetime remains quasi-constant. In this study, the measurements after annealings are performed only at room temperature and consequently, cannot discriminate whether, in this temperature range, negative ions recover or the nature of vacancy-type defects change.

In electron-irradiated 6*H*-SiC material, Polity, Huths, and Lausmann[18] can unambiguously conclude from their lifetime data measured at various temperatures that negative ions anneal out from 480 to 930 °C and divacancies from 930 to 1430 °C without formation of a new type of vacancy-related defect. This last result, obtained in initially $n > 5.4 \times 10^{17}\,\mathrm{cm}^{-2}$ 6*H*-SiC after electron irradiation, is in apparent contradiction with our present results, obtained in initially $n = 10^{17}\,\mathrm{cm}^{-2}$ 6*H*-SiC after proton implantation. However, both results can become consistent when it is noticed that the dopant concentration and the localization of defects initially differ. Defects created along an ion track are initially more localized than those created by electron irradiation. Our conclusion is that the formation of $n \geqslant 3$ small vacancy clusters seems to be possible in 6*H*-SiC when the nitrogen doping is low and the initial distribution of vacancies localized.

After 1300 °C annealing, defects are surviving both in the track region and in the cascade region. If any of them contribute to compensation, one may expect that the carrier profile is inhomogeneous as a function of depth in Smart Cut structures. Annealing has a strong effect in the cascade region, whereas it seems to be rather weak along the track. The contribution of the cascade appears also to be small in the 900 °C as-fractured 6*H*-SiC(*H*sc) and rather strong after the 1300 °C annealing. One could attribute these differences to hydrogen. Hydrogen is mainly located in the cascade region. Its concentration measured by secondary mass spectrometry is still high after 1100 °C annealing[4] and drops to its value before implantation after 1300 °C annealing. Hydrogen plays nearly no role in the track region, whereas it controls what happens in the cascade region. The clusters give a much smaller signal when filled with hydrogen after 900 °C annealing than when empty after hydrogen desorption at 1300 °C. Similar behavior has been well observed in Si implanted with He.[24] The increase in the concentration of open volume defects in He-implanted Si (Ref. 21) detected by positrons correlates to the increase in the fraction of H or He desorbed. It has been observed that, in Si, cavities give a lower *S* when filled with He or H than when they are empty. The desorption and refilling process can be reproduced.[26] In GaAs implanted with 60-keV protons,[27] it has been shown that the presence of hydrogen in the cascade region prevents the positron trapping in the vacancy defects in the cascade region if the hydrogen concentration in the cascade region is sufficiently high.

In our study, when the annihilation characteristics from the vacancy-related defects produced in the track or cascade region are combined to the lattice in 6*H*-SiC, the *S* and *W* data fall on straight lines close to the line joining the Si and

SiC lattice (S,W) points. The annihilation characteristics in Si lattice when compared to those in 6*H*-SiC, $(S(\mathrm{Si}),W(\mathrm{Si}))=(1.15,0.625)$ $(S_{\mathrm{ref}},W_{\mathrm{ref}})$, are of the order of those fitted for the cavities in the cascade region after 1300 °C annealing. Brauer *et al.*[8] report values in 6*H*-SiC, as high as $S=1.19\ S_{\mathrm{ref}}$, after amorphization performed over $\geqslant$120 nm by high-fluence ($\geqslant 3\times10^{18}\,\mathrm{cm}^{-2}$) 200-keV Ge (82-nm) implantation: in this amorphized region positrons lifetime spectra show a lifetime component reaching 305 ps, attributed to vacancies clusters. Our conclusion is that the *S* and *W* values for the Si lattice are of the order of those due to big open-volume defects in SiC.

V. CONCLUSION

In summary, the nature of the vacancy-type defects in 6*H*-SiC after electron or ion implantation suggest that some monovacancies migrate at low temperature ($\ll$25 °C) in 6*H*-SiC. In 6*H*-SiC initially $n=10^{17}\,\mathrm{cm}^{-2}$, nearest-neighbor divacancies seem to be the dominant defects created along the proton track. Annealing at 900 °C produces a new type of defect along the track with positron annihilation characteristics *S* and *W* at least 1.02 and, respectively, 0.9 times the characteristics at divacancies. Cavities in the proton cascade region are well revealed after hydrogen desorption at 1300 °C.

[1] M. Bruel, Electron. Lett. **31**, 1201 (1995).
[2] M. Bruel, Nucl. Instrum. Methods Phys. Res. B **108**, 313 (1996).
[3] L. Di Cioccio, Y. Le Tiec, F. Letertre, C. Jaussaud, and M. Bruel, Electron. Lett. **32**, 1144 (1996).
[4] L. Di Cioccio, Y. Le Tiec, C. Jaussaud, E. Hugonnard-Gruyère, and M. Bruel, Mater. Sci. Forum **264**, 765 (1998).
[5] L. Liszkay, C. Corbel, L. Baroux, P. Hautojärvi, M. Bayhan, A. W. Brinkman, and S. Tatarenko, Appl. Phys. Lett. **64**, 1380 (1994).
[6] A. van Veen, H. Schut, J. de Vries, R. A. Hakvoort, and M. R. Ijpma, in *Positron Beams for Solids and Surfaces*, edited by P. J. Schultz, G. R. Massoumi, and P. J. Simpson (AIP, New York, 1990), p. 171.
[7] J. Mäkinen, P. Hautojärvi, and C. Corbel, J. Phys.: Condens. Matter **4**, 5137 (1992).
[8] G. Brauer, W. Anwand, E. M. Nicht, J. Kuriplach, M. Sob, N. Wagner, P. G. Coleman, M. J. Puska, and T. Korhonen, Phys. Rev. B **54**, 2512 (1996); G. Brauer, W. Anwand, P. G. Coleman, A. P. Knights, F. Plazaola, Y. Pacaud, W. Skorupa, J. Störmer, and P. Willutzki, *ibid.* **54**, 3084 (1996).
[9] S. Dannefaer, W. Puff, and D. Kerr, Phys. Rev. B **55**, 2182 (1997).
[10] J. F. Ziegler and J. P. Biersack, *The Stopping and Range of Ions in Solids* (Pergamon, New York, 1985).
[11] L. A. de S. Balona and J. H. N. Loubser, J. Phys. C **3**, 2344 (1970).
[12] M. O. Aboelfotoh and J. P. Doyle, Phys. Rev. B **59**, 10 823 (1999).
[13] G. Pensl and W. J. Choyke, Physica B **185**, 264 (1993).
[14] H. Itoh, M. Yoshikawa, I. Nashiyama, H. Okumura, S. Misawa, and S. Yshida, J. Appl. Phys. **77**, 837 (1995).
[15] W. J. Choyke, Inst. Phys. Conf. Ser. **31**, 58 (1977).
[16] G. Brauer, W. Anwand, P. G. Coleman, A. P. Knights, F. Plazaola, Y. Pacaud, W. Skorupa, J. Störmer, and P. Willutzki, Phys. Rev. B **54**, 3084 (1996).
[17] A. A. Rempel and H. E. Schäfer, Appl. Phys. A: Mater. Sci. Process. **61**, 51 (1995).
[18] A. Polity, S. Huth, and M. Lausmann, Phys. Rev. B **59**, 10 603 (1999).
[19] W. Puff, P. Mascher, A. G. Balogh, and H. Baumann, Mater. Sci. Forum **258-263**, 733 (1997).
[20] G. Brauer, W. Anwand, E. M. Nicht, J. Kuriplach, M. Sob, N. Wagner, P. G. Coleman, M. J. Puska, and T. Korhonen, Phys. Rev. B **54**, 2512 (1996).
[21] H. Kauppinen, C. Corbel, L. Liszkay, T. Laine, J. Oila, K. Saarinen, P. Hautojärvi, M-F. Barthe, and G. Blondiaux, J. Phys.: Condens. Matter **9**, 10 595 (1997).
[22] J. Mäkinen, C. Corbel, P. Hautojärvi, P. Moser, and F. Pierre, Phys. Rev. B **39**, 10 162 (1989).
[23] M. Hakala, M. J. Puska, and R. M. Nieminen, Phys. Rev. B **57**, 7621 (1998).
[24] R. S. Brusa, G. P. Karwasz, N. Tiengo, A. Zecca, F. Corni, G. Calzolari, and C. Nobili, J. Appl. Phys. **85**, 2390 (1999).
[25] E. Soininen, J. Mäkinen, D. Beyer, and P. Hautojärvi, Phys. Rev. B **46**, 13 104 (1992).
[26] A. van Veen, R. A. Hakvoort, H. Schut, and P. E. Mijnarends, J. Phys. IV **1**, 37 (1995).
[27] K. Saarinen, P. Hautojärvi, J. Keinonen, E. Rauhala, J. Raïsänen, and C. Corbel, Phys. Rev. B **43**, 4249 (1991).